J Fusion Energ (2013) 32:42–49
DOI 10.1007/s10894-012-9522-8

ORIGINAL RESEARCH

Numerical Experiments on Radiative Cooling and Collapse in Plasma Focus Operated in Krypton

S. Lee · S. H. Saw · Jalil Ali

Published online: 26 February 2012

Abstract The Plasma Focus has wide-ranging applications due to its intense radiation of SXR, XR, electron and ion beams and fusion neutrons when operated in deuterium. The 5-phase Lee Model code has been developed for the focus operated in various gases including D, D–T, He, Ne, N, O, Ar, Kr and Xe. Radiation-coupled motion is included in the modelling. In this paper we look at the effect of radiation cooling and radiation collapse in krypton. The Pease–Braginskii current is that current flowing in a hydrogen pinch which is just large enough for the Bremsstrahlung to balance Joule heating. This radiation-cooled threshold current for a hydrogen pinch is 1.6 MA. It is known that in gases undergoing line radiation strongly the radiation-cooled threshold current is considerably lowered. We show that the equations of the Lee Model code may be used to compute this lowering. The code also shows the effect of radiation cooling leading to radiative collapse. Numerical experiments based on experimentally fitted model parameters are run to demonstrate a regime in which radiation collapse is observed in Kr at a pinch current of 50–100 kA.

S. Lee · S. H. Saw
INTI International University, 71800 Nilai, Malaysia
e-mail: sorheoh.saw@newinti.edu.my

S. Lee (✉) · S. H. Saw
Institute for Plasma Focus Studies, 32 Oakpark Drive, Chadstone, Australia
e-mail: leesing@optusnet.com.au

J. Ali
Institute of Advanced Photonic Science, Nanotechnology Research Alliance, Universiti Teknologi Malaysia, 81310 Johor Baru, Malaysia
e-mail: djxxx_1@yahoo.com

Keywords Plasma focus · Plasma focus modeling · Radiative cooling · Radiative collapse · Plasma focus radiation

Introduction

The Plasma Focus has wide-ranging applications due to its intense radiation of SXR, XR, electron and ion beams, and fusion neutrons [1] when operated in deuterium. The use of gases such as Ne and Xe for generation of specific SXR or EUV lines for micro-lithography applications [2] has been widely discussed in the literature as has the use of N and O to generate the lines suitable for water-window microscopy [3]. Recently Ar has been considered for micro-machining due to the harder characteristic line radiation [4]. Various gases including Kr have been discussed and used for fusion neutron yield enhancement [5] due arguably to mechanisms such as thermodynamically enhanced pinch compressions.

The possibility of intense radiation leading to extreme compressions in a Z pinch and the implications of such a mechanism for development of radiation sources has recently been reviewed [6]. Shearer [7] considered an equilibrium model of the Z pinch based on Bennett relation, radiation losses and Ohmic heating to explain the highly localized x-ray sources observed in plasma focus experiments. Vikhrev [8] considered the dynamics of a Z pinch contraction in deuterium with appreciable radiative loss taking into account decreased current due to pinch inductance and resistance; the viscous heat and anomalous resistive heat release, transition of plasma Bremsstrahlung into blackbody surface radiation, the pressure of the degenerate electron gas and the thermonuclear heat release. A neutron yield of 10^{14} is found from a highly compressed

plama of a 2 MJ system. With a 1% mixture of xenon with a fully ionized plasma at 10 MA the enhanced compression to a density of 10^{27} cm^{-3} leads to a neutron yield of 1.5×10^{16}. Using a mixture of deuterium and tritium the neutron yield reached 10^{18} per discharge with input energy of 2 MJ, reaching breakeven according to their calculations. Koshelev et al. [9] considered the formation of radiation enhanced micropinches as a source of highly ionized atoms.

In this paper we look at the effect of radiation cooling and radiation collapse in krypton. The Pease–Braginskii current [10, 11] is known to be that current flowing in a hydrogen pinch which is just large enough for the Bremsstrahlung to balance Joule heating. This radiation-cooled threshold current for a hydrogen pinch is 1.6 MA. It is known that in gases undergoing line radiation strongly the radiation-cooled threshold current is considerably lowered [12].

We show that the equations of the Lee Model code [13] may be used to compute this lowering. The model is correctly coupled between the plasma dynamics and the electrical circuit which is an advantageous feature when compared to computations which use a fixed current or a current which is not correctly associated with the electric circuit interacting with the plasma dynamics. The model treats the pinch as a column. Our computations show that the radial collapse of the column is significantly enhanced by the net energy loss due to radiation and joule heating with consideration of plasma opacity. This radiatively enhanced compression of the plasma column would in reality mean that as the column breaks up into localized regions (hot spots) radiative collapse would be further enhanced. Thus the calculated radiative collapse of the column would be an underestimate of the more realistic 'line of hot spots' situation. Nevertheless the Lee code does give useful information since it incorporates the time history of the axial and radial phases. Earlier work [8] has already suggested that the neutron enhancement effect of seeding [5] could at least in part be due to the enhanced compression caused by radiation cooling.

We discuss here the 5-phase Lee Model code for the focus operated in Kr. A corona model is used to generate the thermodynamic data required in the computation.

The Lee Model Code

The Lee model code couples the electrical circuit with plasma focus dynamics, thermodynamics, and radiation, enabling a realistic simulation of gross focus properties. The basic model [14] was successfully used for several projects [15–18]. Radiation-coupled dynamics was included, leading to numerical experiments on radiation cooling [19]. The vital role of a finite small disturbance speed [20] was incorporated together with real gas thermodynamics and radiation-yield terms. This version assisted other projects [17–21] and was web published [22] with plasma self-absorption included in 2007 [22], improving the SXR yield simulation. The code has been used in several machines including UNU/ICTP PFF [2, 17–19, 22–26], NX2 [2, 4, 21, 27], and NX1 [2] and has been adapted for the Filippov-type plasma focus DENA [28]. A recent development includes neutron yield Y_n using a beam–target mechanism [29–33], incorporated in recent versions [13] of the code (after RADPFV5.13), resulting in realistic Y_n scaling with I_{pinch} [34–36]. The versatility of the model is demonstrated in its distinction of I_{pinch} from I_{peak} [31] and the recent uncovering of a pinch current limitation effect [32, 33], as static inductance is reduced towards zero. Numerical experiments uncovered neutron [29, 30, 34] and SXR [36–39] scaling laws over a wider range of energies and currents than attempted before and gave insight into the nature and cause of 'neutron saturation' [34].

A brief description of the 5-phase model is given in the following.

The 5 Phases

The five phases (*a–e*) are summarised [13, 39] as follows:

a. Axial Phase (see Fig. 1 *left part):* Described by a snowplow model with an equation of motion which is coupled to a circuit equation. The equation of motion incorporates the axial phase model parameters: mass and current factors f_m and f_c. The mass swept-up factor [40] f_m accounts for the porosity of the current sheet, the inclination of the current sheets-shock front structure, boundary layer and all other unspecified effects which changes the amount of mass in the moving structure. The current factor f_c accounts for the fraction of current effectively flowing in the moving structure due to all effects such as current shedding and current sheet inclination.

b. Radial Inward Shock Phase (see Fig. 1 *right part)*: Described by 4 coupled equations using an elongating slug model. The first equation computes the radial inward shock speed from the driving magnetic pressure. The second computes the axial column elongation speed. The third computes the speed of the current sheath (magnetic piston), allowing the sheath to separate from the shock front [20]. The fourth is the circuit equation. Thermodynamic effects due to ionization and excitation are incorporated. Temperature and number densities are computed using shock-jump equations. The model parameters, radial phase mass swept-up and current factors f_{mr} and f_{cr} are incorporated in all three radial phases.

c. Radial Reflected Shock (RS) Phase: When the shock front hits the axis, because the plasma is collisional, a

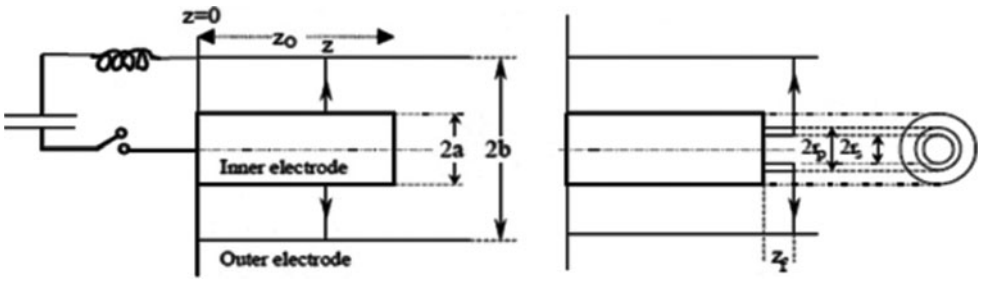

Fig. 1 Schematic of the axial and radial phases. The left section depicts the axial phase, the right section the radial phase. In the left section, z is the effective position of the current sheath-shock front structure. In the right section r_s is the position of the inward moving shock front driven by the piston at position r_p. Between r_s and r_p is the radially imploding slug, elongating with a length z_f. The capacitor, static inductance and switch powering the plasma focus is shown for the axial phase schematic only

reflected shock develops which moves radially outwards, whilst the radial current sheath continues to move inwards. Four coupled equations are used, these being for the reflected shock moving radially outwards, the piston moving radially inwards, the elongation of the annular column and the circuit. The plasma temperature behind the reflected shock undergoes a jump by a factor of 2. Number densities are computed using reflected shock jump equations.

d. Slow Compression (Quiescent) or Pinch Phase: When the out-going reflected shock hits the inward moving piston, the compression enters a radiative phase. For gases such as neon, radiation emission may enhance the compression as energy loss/gain terms from Joule heating and radiation are included in the piston equation of motion. Three coupled equations are used; these being for piston radial motion, pinch column elongation and for the circuit. The duration of this slow compression (pinch) phase is set as the time of transit of small disturbances across the pinched plasma column. The gross column is considered not including the effects of localized regions of high densities and temperatures [41].

e. Expanded Column Axial Phase: To simulate the current trace beyond this point we allow the column to suddenly attain the radius of the anode, and use the expanded column inductance for further integration. This phase is not considered important as it occurs after the focus pinch.

Radiation Cooling and Collapse in Krypton

We look at the thermodynamic processes in krypton as it is heated to high temperatures.

The ionization curves of Kr are computed from the corona model [42] using ionization data [43]. From these ionization curves the effective charge Z_{eff} and the specific heat ratio γ of Kr are computed [44].

The Pease–Braginskii P–B current [10, 11] is the value of current (1.6 MA) at which the Bremsstrahlung (considered as a loss from the plasma) equals the Joule heating of the plasma pinch column in hydrogen assuming Spitzer resistivity. When pinch current exceeds this value, the Bremsstrahlung losses exceed Joule heating and the plasma pinch begins to experience increasingly severe radiative cooling effects at progressively higher currents until radiative collapse may be observed. The P–B current only considers Bremsstrahlung, since at the high temperatures experienced in the hydrogen or deuterium pinch, the gases are fully ionized and there is no line radiation.

For gases such as neon, argon, krypton and xenon, there may still be line radiation even at the high pinch temperatures. This line radiation may considerably exceed the effect of Bremsstrahlung. In that case, the effect of radiation cooling, and eventually radiative collapse may be exacerbated; and may occur at much lower currents [45].

Power Balance

We consider the following powers (all quantities in SI units unless otherwise stated): respectively Joule heating, Bremsstrahlung and Line radiation generated in a plasma column of radius r_p, length l at temperature T:

$$\frac{dQ_J}{dt} = C_J T^{-3/2} \frac{l}{\pi r_\rho^2} Z_{eff} I^2 \quad \text{where } C_J \cong 1300 \quad \text{Zn is atomic number and } T \text{ is in Kelvin} \tag{1}$$

$$\frac{dQ_{Brem}}{dt} = C_1 T^{1/2} n_i^2 Z_{eff}^3 \pi r_p^2 l \quad \text{where } n_i \text{ is in m}^{-3} \text{ and } C_1 = 1.6 \times 10^{-40} \tag{2}$$

$$\frac{dQ_{line}}{dt} = C_2 T^{-1} n_i^2 Z_n^4 Z_{eff} \pi r_p^2 l \quad \text{where } C_2 = 4.6 \times 10^{-31} \tag{3}$$

We use the Bennett distribution to obtain a relationship between T (pinch temperature) and I (pinch current) as follows:

$$T = b\frac{I^2}{\left(n_i r_p^2\right)\left(1+Z_{eff}\right)} \quad \text{where } b = \frac{\mu}{8\pi^2 k} \tag{4}$$

So that we write the total power adding the three terms as follows:

$$\frac{dQ}{dt} = -\pi\left[C_1 b^{1/2}\right]\frac{Z_{eff}^3}{\left(1+Z_{eff}\right)^{1/2}} n_i^{3/2} r_p l I - \frac{\pi C_2}{b}\left(1+Z_{eff}\right) Z_{eff} Z_n^4 n_i^3 r_p^4 \frac{l}{I^2} + \frac{C_J}{\pi b^{3/2}}\left(1+Z_{eff}\right)^{3/2} Z_{eff} n_i^{3/2} r_p \frac{l}{I} \tag{5}$$

In the above μ = permeability k = Boltzmann Constant, Z_n = atomic number and n_i = ion number density.

Check Equation (5) for the Value of Pease–Braginskii Current I_{P-B}

From (5) if we consider only the two terms, Joule heating power and the Bremsstrahlung power; then putting that version of (5) to zero we obtain the threshold current as:

$$I_{p-B}^2 = \frac{C_J}{C_1\pi^2 b^2}\frac{\left(1+Z_{eff}\right)^2}{Z_{eff}^2} = \frac{4C_J}{C_1\pi^2 b^2} \tag{6}$$

Noting that for hydrogen $Z_{eff} = 1$; and I_{P-B} computes correctly to a value of 1.6 MA.

Line Radiation Greatly Reduces the Threshold Current

Considering the general case with all three power terms of (5) we obtain:

$$I^2 = \frac{C_J\left(1+Z_{eff}\right)^2}{C_1\pi^2 b^2 Z_{eff}^2} \times \frac{C_1 Z_{eff}^2}{\left[C_2 z_n^4 T^{-3/2} + C_1 Z_{eff}^2\right]} \tag{7}$$

So that we may write:

$$I^2 = \frac{I_{P-B}^2}{4} \times \frac{1}{\left[\frac{C_2 z_n^4 T^{-3/2}}{C_1 Z_{eff}^2} + 1\right]} \times \frac{\left(1+Z_{eff}\right)^2}{Z_{eff^2}} \tag{8}$$

or

$$I^2 = I_{P-B}^2 \times \frac{1}{K} \tag{9}$$

where

$$K = 4\left[\frac{(dQ_{line}/dt) + (dQ_{Brem}/dt)}{(dQ_{Brem}/dt)}\right] \tag{10}$$

Note that in (8) above the factor $Z_{eff}^2/(1+Z_{eff})^2 \sim 1$ since Z_{eff} has the value >10 for typical plasma focus operation in Ar, Kr and Xe; and with this approximation (9) holds.

For (10) in plasma focus operation in Kr, typically in the range 100 to 1,000 eV, the ratio $[dQ_{line}/dt/dQ_{Brem}/dt]$ has the range 1,000 times to 10 times; so the threshold current is reduced from I_{P-B} by a factor of ~30 at 100 eV to ~3 times at 1,000 eV; i.e to ~50 kA at 100 eV and to ~500 kA at 1,000 eV. In other words at the lower temperature end of plasma focus operation in Kr a current of 50 kA may be enough to reach the threshold at which line radiation begins to exceed joule heating.

Summarising: This greatly-reduced threshold current is reflected in (9) where the reduction factor K is seen in (10) to be a large factor since line radiation greatly exceeds Bremsstrahlung.

Effect of Plasma Self-Absorption

We also note that the above consideration has not taken into account the effect of plasma self-absorption. Taking that into consideration the emission power will be reduced, effectively reducing the value of K thus raising the threshold current from that value computed in (9).

The Lee Model code incorporates radiation-coupled dynamics [13] using the following equation:

$$\frac{dr_p}{dt} = \frac{\frac{-r_p}{\gamma I}\frac{dI}{dt} - \frac{1}{\gamma+1}\frac{r_p}{Z_f}\frac{dZ_f}{dt} + \frac{4\pi(\gamma-1)}{\mu\gamma Z_f}\frac{r_p}{f_c^2 I^2}\frac{dQ}{dt}}{\frac{\gamma-1}{\gamma}} \tag{11}$$

where dQ/dt is computed from (5).

Plasma self-absorption [13, 46–48] is included by computing the value of plasma self-absorption correction factor A_{ab}:

$$A_{ab} = [(1 - 10_{-20} n_i Z_{eff})]^{-(1+M)} \tag{12}$$

where T_{ev} is the temperature in eV and M is the photonic excitation number:

$$M = 1.66 \times 10^{-15} r_p Z_n^{1/2} n_i / (Z_{eff} T_{\mathrm{eV}}^{1.5}) \tag{13}$$

When there is no plasma self-absorption $A_{ab} = 1$. When A_{ab} goes below 1, plasma self absorption starts. When a sizeable fraction of the photons is re-absorped e.g. value of A_{ab} reaches 1/e, plasma radiation is considered to switch over from volume radiation to surface radiation and is computed accordingly in the model.

Summarizing: The code computes the amount of radiation emitted, computes plasma self absorption effects and incorporates these effects into the plasma dynamics.

Numerical Experiment in Krypton Demonstrating Radiative Collapse

The UNU ICTP PFF [17] has the following parameters: capacitance $C_0 = 30$ μF, static inductance $L_0 = 114$ nH, 13 mΩ resistance, $b = 3.2$ cm, $a = 0.95$ cm, $z_0 = 16$ cm. A series of shots were fired in krypton at pressures ranging

from 0.1 to 1.5 Torr using the INTI PF [39, 49–51] which is an identical machine. Current fitting was carried out from which we deduce fitting parameters of $f_m = 0.035$, $f_c = 0.7$, $f_{mr} = 0.1$, $f_{cr} = 0.7$. A typical shot is shown in Fig. 2; showing a typically good fit.

Recent experimental measurements on neon and argon over a range of pressures on the INTI PF and the Syrian SYPF-2 [50] have shown that the axial phase mass factor f_m for neon is 0.04 ± 0.01 over an operational range of 0.7–4 Torr and argon 0.05 ± 0.01 over 0.2–1.2 Torr. Thus we have experimental confirmation that over a range of operating pressures we may reasonably take an average representative value for f_m. We also have fitted radial phase model parameters for a wide range of conditions for deuterium, neon and argon. These show that when the pressure is within the range so that the radial phase starts near the peak current then the radial phase model parameters are also within a very narrow range so that a representative value may be taken. But when the radial phase starts too far away from the peak current (for example at times greater than 4 μs for a machine with risetime to peak current of 3 μs) then the radial mass factor may vary over a substantial range. In order to run numerical experiments in Kr over a range of pressures we fire some shots in Kr over a range of pressures from 0.1 to 1.5 Torr and determined that over the whole range we may take a representative value of $f_m = 0.035$ $fc = 0.7$, $f_{cr} = 0.7$; whereas for the radial mass factor representative value of 0.1 is taken for the range 0.1–0.75 Torr and 0.2 is taken for the range of 1–1.5 Torr. Having thus obtained experimentally fitted model parameters we ran numerical experiments with the INTI PF in Kr over 0.1–1.5 Torr.

The radial trajectories are shown in Fig. 3a–g.

It is clear from Fig. 3 that radiative cooling reduces the pinch radius as pressure is increased, above 0.5 Torr. Strong radiative collapse is evident in the range 0. 75–1.25 Torr (Fig. 3d, e).

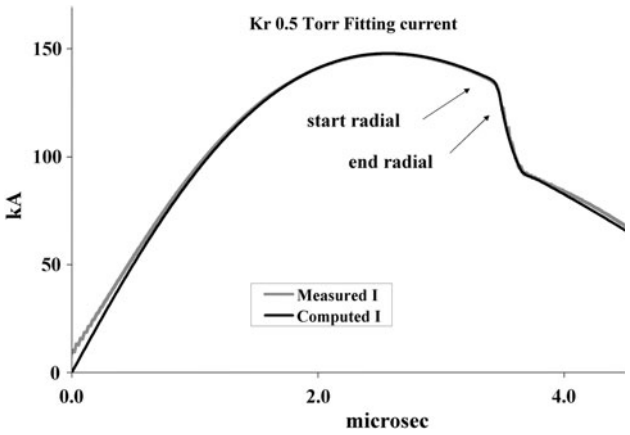

Fig. 2 Current trace (measured) for krypton at 12 kV 0.5 Torr INTI PF used to fit computed current trace. The good fit is obtained with fitted parameters: $f_m = 0.035$, $f_c = 0.7$, $f_{mr} = 0.09$ $f_{cr} = 0.7$

Figure 3a acts as a reference situation and shows the radial dynamics at 0.1 Torr. The radial inward shock wave starts at 9.5 mm and is driven to the axis after 34 ns with the driving magnetic piston trailing it by some 1.5 mm as the shock front hits the axis. A reflected shock RS goes outwards and after some 7 ns hits the incoming piston. At this time the pinch starts and the column compresses inwards a little (as is typical) to a minimum radius of 1 mm. Computed data indicates that in this shot the radiation power emitted (mostly line) is less than the Joule heating power with the pinch temperature in this shot reaching 2.4 keV. Increasing the pressure to 0.25 Torr, the pinch radius is compressed a little more to 0.9 mm.

At 0.5 Torr and a pinch temperature of 630 eV (see Fig. 5) with a pinch current of 94 kA (see Fig. 4), radiative collapse is now significant (see Fig. 3c) with the radius collapsing in 7.5 ns to 0.6 mm. At 0.75 Torr with a pinch temperature of 380 eV and a pinching current 84 kA, the radiative collapse is very strong the collapse going down to a radius of 0.11 mm in 2 ns.

At 1 Torr with a pinch temperature of 132 eV, the collapse does not reach the cut-off radius. In this case the pinch maintains a small radius (0.2 mm) for 13 ns. These are the conditions (high density, relatively long pinch duration) which produce huge line yields of more than 100 J. At 1.25 Torr and pinch temperature of 77 eV with a pinch current of 52 kA, the speeds are much slower now and the pinch occurs late so the current has dropped considerably reducing the pinching force; the radiative collapsed radius is now bigger (0.5 mm).

Finally at 1.5 Torr, the radial phase starts very late at 4.9 μs (peak circuit current is at 2.9 μs) and takes 0.4 μs to reach the pinch phase; by which time the circuit current has dropped to 46 kA way below its peak of 168 kA. The Ipinch is only 32 kA.There is insufficient pinching force and the column blows out instead of pinching in as the RS hits the piston.

From each of the shots (numerical experiment) shown in Fig. 3 is also recorded computed data of that shot including energy distributions and plasma properties. Some of the data is collected in the following Figures. Figures 4, 5 and 6 show the pinch radius, I_{peak} and I_{pinch} and pinch temperature. Other data not shown includes charge number Z_{eff} which reduces from 30 at 0.1 Torr to 10 at 2 Torr. It is clear from Fig. 3 that radiative cooling reduces the pinch radius as pressure is increased above 0.25 Torr. Strong radiative collapse is evident in the range 0.5–1.25 Torr with the radius dropping to the 0.01 'a' cut-off radius imposed in the model.

Figure 5 shows that I_{peak} keeps rising from just 132 kA at 0.1 Torr to 158 kA at 1.5 Torr due to the reduced dynamic resistance loading of the slowing current sheet on the circuit. However I_{pinch} rises from 90 kA at 0.1 Torr

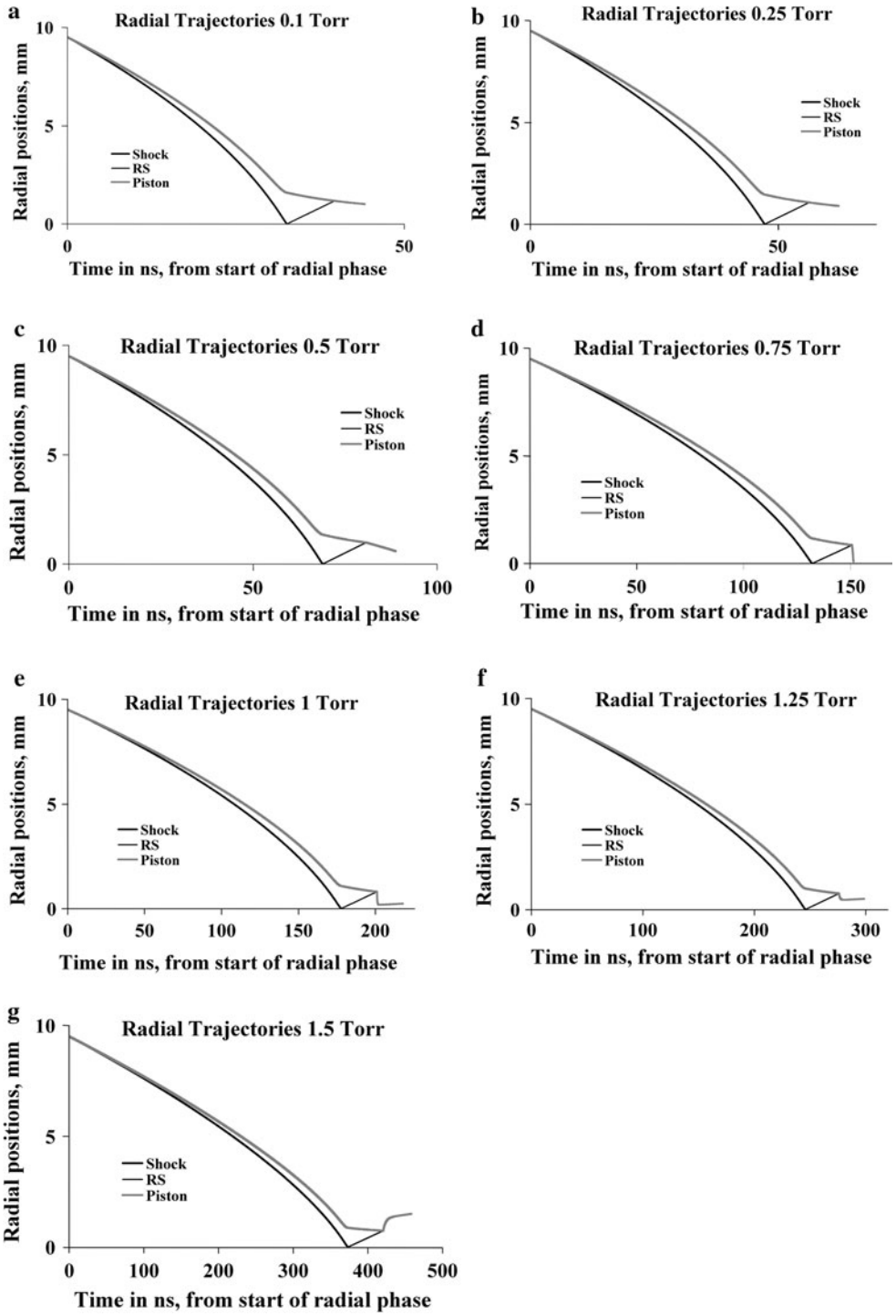

Fig. 3 **a** Radial trajectories at Kr 0.1 Torr, **b** Radial trajectories at Kr 0.25 Torr, **c** Radial trajectories at Kr 0.5 Torr, **d** Radial trajectories at Kr 0.75 Torr, **e** Radial trajectories at Kr 1 Torr, **f** Radial trajectories at Kr 1.25 Torr, **g** Radial trajectories at Kr 1.5 Torr

reaching a maximum around 98 kA at 0.25 Torr then dropping with pressure to 94 kA at 0.5 Torr until it is only 32 kA at 1.5 Torr. The primary reason is the time matching of the pinch with the current risetime of the circuit. At 0.25 Torr the radial phase starts at 2.66 μs with pinch occurring at 2.72 μs which is just before the $(\pi/2)(L_0\,C_0)^{0.5}$ current rise time of 2.86 μs. At 0.5 Torr the radial phase starts at 3.4 μs which is significantly after the time of peak current. At 1 Torr radial phase starts at 4.2 μs with pinch occurring just after 4.3 μs when the circuit current has dropped to 100 kA from a peak value of 156 kA. That explains why the pinch current is only 69 kA despite the increasing value of the peak current. At 1.5 Torr the pinch comes very late at 5.2 μs when the circuit current has already dropped to below 50kA driving the pinch with only 32 kA.

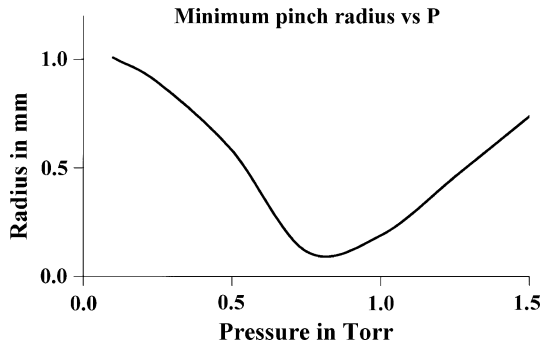

Fig. 4 Minimum pinch radius versus pressure

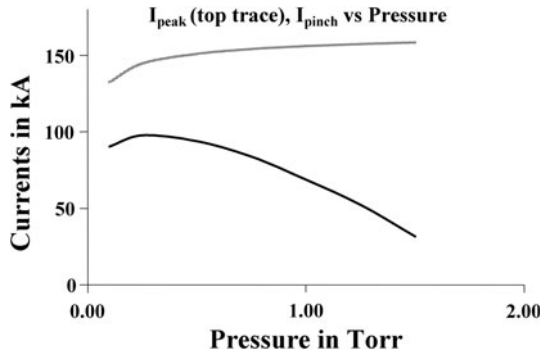

Fig. 5 I_{peak}, I_{pinch} versus pressure

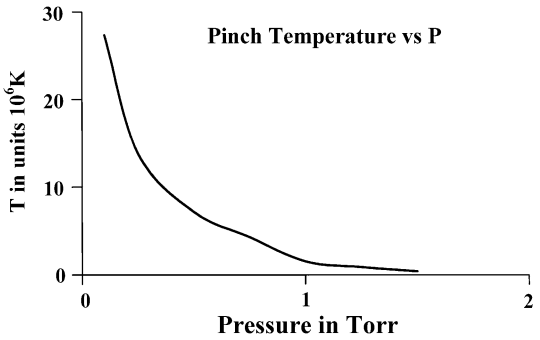

Fig. 6 Pinch temperature versus pressure

The reducing speed of the current sheet and the increasing mismatch of the pinching time to the time of peak current are largely responsible for the behavior of the pinch temperature dropping from 2.4 keV to 77 eV as pressure increases from 0.1 to 1.5 Torr as shown in Fig. 6.

Conclusion

The Lee Model code includes the effect of energy gain/loss into its dynamics, moreover incorporates the effect of plasma self-absorption. Current waveforms were obtained from a series of experiments from 0.1 to 1.5 Torr in krypton with the 3 kJ INTI PF. These current waveforms were fitted to computed current waveforms using the Lee Model code. From the fitting model parameters of mass factors and current factors were found. The code was run in Kr and demonstrates radiative cooling leading to radiative collapse at a pinch current ranging from 50 to 100 kA.

References

1. A. Bernard, H. Bruzzone, P. Choi, H. Chuaqui, V. Gribkov, J. Herrera, K. Hirano, A. Krejci, S. Lee, C. Luo, F. Mezzetti, M. Sadowski, H. Schmidt, K. Ware, C.S. Wong, V. Zoita, Moscow J. Phys. Soc. **8**, 93–170 (1998)
2. S. Lee, P. Lee, G. Zhang, X. Feng, V.A. Gribkov, M. Liu, A. Serban, T. Wong, IEEE Trans. Plasma Sci. **26**, 1119–1126 (1998)
3. R. Lebert, W. Neff, D. Rothweiler, J. X-Ray Sci. Technol. **6**, 2 (1996)
4. V.A. Gribkov, A. Srivastava, P.C.K. Lee, V. Kudryashov, S. Lee, IEEE Trans. Plasma Sci. **30**, 1331–1338 (2002)
5. Rishi. Verma, P. Lee, S. Lee, S.V. Springham, T.L. Tan, R.S. Rawat, M. Krishnan, Appl. Phys. Lett. **93**, 101501 (2008)
6. M.G. Haines. Plasma Phys. Control. Fusion **53**, 093001 (2011). doi:10.1088/0741-3335/53/9/093001
7. J.W. Shearer, Phys. Fluids **19**, 1426 (1976). doi:10.1063/1.861627
8. V. Vikhrev. Pis'ma Zh Elsp Teor Fiz **27**(2), 104–107 (1978)
9. K.N. Koshelev, Yu.V. Sidelnikov, Nucl. Instrum. Methods Phys. Res. **B9**, 204–205 (1985)
10. R. Pease, Procs. Phys. Soc. **70**, 11 (1957)
11. S. Braginskii, Zh. Eksp. Teor. Fiz. **33**, 645 (1957)
12. K.N. Koshelev, V.I. Krauz, N.G. Reshetniak, R.G. Salukvadze Yu, V. Sidelnikov, E.Yu. Khautiev, J. Phys. D Appl. Phys. **21**, 1827 (1988)
13. Lee S. Radiative Dense Plasma Focus Computation Package: RADPF
14. http://www.plasmafocus.net (2011)
15. S. Lee, in *Radiations in Plasmas* Vol II, ed. by B. McNamara (World Scientific, Singapore, 1984) pp. 978–987
16. T.Y. Tou, S. Lee, K.H. Kwek, IEEE Trans. Plasma Sci. **17**, 311–315 (1989)
17. S. Lee, IEEE Trans. Plasma Sci. **19**, 5 (1991)
18. S. Lee, T.Y. Tou, S.P. Moo, M.A. Eissa, A.V. Gholap, K.H. Kwek, S. Mulyodrono, A.J. Smith, S. Suryadi, W. Usada, M. Zakaullah, Am. J. Phys. **56**, 62–68 (1988)
19. S. Lee, A. Serban, IEEE Trans. Plasma Sci. **24**, 1101–1105 (1996)
20. A. Jalil bin. *Development and studies of a small plasma focus*, Ph.D. Dissertation; Universiti Teknologi Malaysia, Malaysia, 1990
21. D.E. Potter, Nucl. Fusion **18**, 813–823 (1978)
22. S. Bing, *Plasma dynamics and X-ray emission of the plasma focus* (Nanyang Technological University, Singapore, Ph.D. dissertation, 2000)
23. A. Serban, S. Lee, J. Plasma Phys. **60**, 3–15 (1998)
24. M.H. Liu, X.P. Feng, S.V. Springham, S. Lee. IEEE Trans. Plasma Sci., **26**, 135 (1998)
25. S. Lee, *Twelve years of UNU/ICTP PFF—a review*. Abdus Salam ICTP, Trieste IC/98/231, p 5–34, (1998)
26. S.V. Springham, S. Lee, M.S. Rafique. Plasma Phys. Control. Fusion, **42**, 1023 (2000)

27. Lee S. (2010) [Online]. Available: http://ckplee.myplace.nie.edu.sg/plasmaphysics/
28. D. Wong, P. Lee, T. Zhang, A. Patran, T.L. Tan, R.S. Rawat, S. Lee, Plasma Sources Sci. Technol. **16**, 116–123 (2007)
29. V. Siahpoush, M.A. Tafreshi, S. Sobhanian, S. Khorram, Plasma Phys. Control. Fusion **47**, 1065–1075 (2005)
30. S. Lee, S.H. Saw, J. Fusion Energ. **27**, 292–295 (2008)
31. S. Lee, Plasma Phys. Control. Fusion **50**(105), 005 (2008)
32. S. Lee, S.H. Saw, P.C.K. Lee, R.S. Rawat, H. Schmidt, Appl. Phys. Lett. **92**(111), 501 (2008)
33. S. Lee, S.H. Saw, Appl. Phys. Lett. **92**(021), 503 (2008)
34. S. Lee, P. Lee, S.H. Saw, R.S. Rawat, Plasma Phys. Control. Fusion **50**, 065012 (2008)
35. S. Lee, Appl. Phys. Lett. **95**, 151503 (2009)
36. S. Lee, S.H. Saw, L. Soto, S.P. Moo, S.V. Springham, Plasma Phys. Control. Fusion **51**, 075006 (2009)
37. S. Lee, S.H. Saw, P. Lee, R.S. Rawat, Plasma Phys. Control. Fusion **51**, 105013 (2009)
38. M. Akel, Sh. Al-Hawat, S.H. Saw, S. Lee, J. Fusion Energy **29**, 223–231 (2010)
39. S. Lee, R.S. Rawat, P. Lee, S.H. Saw, J. Appl. Phys. **106**, 023309 (2009)
40. S.H. Saw, P.C.K. Lee, R.S. Rawat, S. Lee, IEEE Trans. Plasma Sci. **37**, 1276 (2009)
41. S.P. Chow, S. Lee, B.C. Tan, J. Plasma Phys. **8**, 21–31 (1973)
42. M. Favre, S. Lee, S.P. Moo, C.S. Wong, Plasma Sources Sci. Technol. **1**, 122 (1992)
43. McWhirter in *Plasma diagnostic techniques* ed. by R. Huddelstone, S.L. Leonard (Academic Press, New York, 1965)
44. http://physics.nist.gov/PhysRefData/Elements/
45. S. Lee, Aust. J. Phys. **35**, 391 (1983)
46. K. Koshelev, N. Pereira, J. Appl. Phys. **69**, 21–44 (1991)
47. A.E. Robson. Phys. Fluid **B3**, 1481 (1991)
48. N.A.D. Khattak Anomalous Heating (LHDI). http://www.plasmafocus.net/IPFS/modelpackage/File3Appendix.pdf (2011)
49. S.H. Saw, S. Lee, F. Roy, P.L. Chong, V. Vengadeswaran, A.S.M. Sidik, Y.W. Leong, A. Singh, Rev. Sci. Instrum. **81**, 053505 (2010)
50. S. Lee, S.H. Saw, R.S. Rawat, P. Lee, R. Verma, A. Talebitaher, S.M. Hassan, A.E. Abdou, I. Mohamed, M. Amgad, H. Torreblanca, Sh. Al Hawat, M. Akel, P.L. Chong, F. Roy, A. Singh, D. Wong, K. Devi. J. Fusion Energy (2011) Online First™ 27 July. doi:10.1007/s10894-011-9456-6
51. Sh. Al-Hawat, M. Akel, S. Lee, S.H. Saw, J. Fusion Energ. **31**, 13–20 (2012)